Journal of Hazardous Materials 175 (2010) 524–531

Contents lists available at ScienceDirect

Journal of Hazardous Materials

journal homepage: www.elsevier.com/locate/jhazmat

Photoelectrocatalytic properties of nitrogen doped TiO_2/Ti photoelectrode prepared by plasma based ion implantation under visible light

Lei Han[a], Yanjun Xin[a,c], Huiling Liu[a,*], Xinxin Ma[b], Guangze Tang[b]

[a] State Key Laboratory of Urban Water Resources and Environment (SKLUWRE), Department of Environmental Science and Engineering Harbin Institute of Technology, Huanghe Road 73, Nangang District, Harbin 150090, China
[b] State Key Lab of Advanced Welding Technology, Harbin Institute of Technology, Weat Dazhi St. 91, Nangang District, Harbin 15001, China
[c] School of Resource and Environment, Qingdao Agricultura1 University, Qingdao 266109, China

ARTICLE INFO

Article history:
Received 13 August 2009
Received in revised form 8 October 2009
Accepted 10 October 2009
Available online 20 October 2009

Keywords:
TiO_2/Ti photoelectrode
Anodization
Plasma based ion implantation (PBII)
Nitrogen
Photoelectrocatalysis

ABSTRACT

Nitrogen doped TiO_2/Ti photoelectrodes were prepared by a sequence of anodization and plasma based ion implantation (PBII). The properties of this photoelectrode were characterized by scanning electronic microscopy (SEM), atomic force microscopy (AFM), X-ray diffraction (XRD), X-ray photoelectron spectrometry (XPS), Ultra violet/visible light diffuse reflectance spectra (UV/vis/DRS), surface photovoltage (SPV), etc. Photoelectrocatalytic (PEC) performance of N-doped TiO_2/Ti photoelectrode was tested under visible light irradiation. Their photocatalytic activity was evaluated by degradation of Rhodamine B (Rh.B). The results of XPS showed that nitrogen element was in form of three species, i.e. β-N, molecular γ-N and O–Ti–N, which existed in the lattices of TiO_2 and gaps between molecules. The results of UV/vis/DRS spectra and SPV revealed that proper doping of nitrogen could expand the response of photoelectrodes towards visible light and diminish the recombination of photo-generated holes and electrons, respectively. The photoelectrocatalytic activity of N-doped TiO_2/Ti photoelectrodes was superior to those of undoped one under visible light region irradiation.

1. Introduction

Since the discovery of water splitting on TiO_2 surfaces by photo-irradiation, TiO_2 has attracted extensive interest. In the past three decades, titanium dioxide has been extensively studied throughout the world and considered as promising photocatalyst in the degradation of organic pollutants, sewage treatment, and disinfection due to its superior photocatalytic activity [1–6], which can decompose organic contaminants in wastewater to CO_2 and H_2O effectively, as well as eliminate hazardous gases in atmosphere [7].

Unfortunately, TiO_2 photocatalyst has a band gap of 3.2 eV, and can only be activated by UV radiation ($\lambda < 387$ nm) that constitutes only a small fraction (3–5%) of the solar spectrum. Thus, the use of visible light (400–750 nm), which constitutes ~45% of the solar spectrum, is limited due to its wide band gap [8]. In addition, the high recombination rate of electron–hole pairs on the surface and in the bulk phase of TiO_2, and the low quantum yield holds back its practical applications as photocatalytic materials [9].

Therefore, developing a novel method that provides photocatalyst with sufficient photosensitivity in the visible light region has been the major research effort in the recent years. For this purpose, many methods have been investigated, including transition metal and rare earth element doping, noble metal deposition, semiconductor coupled and dye sensitization, etc [10–14]. Recently, it has been found that TiO_2 doped with some elements such as N, S, F and C would extend the photoactive region to the visible light. Nitrogen doping seems to be more attractive among all of these anionic elements due to its comparable atomic size with oxygen, small ionization energy, metastable center formation and stability [15]. Among the nonmetals (C, N, F, P and S) studied for doping, theoretical calculations predicted an ideal band-gap control for N-doping of TiO_2 was the same as the experimental results, which showed promising photocatalytic activity [8]. Pelaez et al. prepared N/F codoped TiO_2 nanoparticles by a sol–gel method and degrade microcystin-LR in water [16]. Livraghi et al. also proposed that nitrogen species involved in N–TiO_2 was responsible for visible light absorption for promotion of electrons from the band gap localized states to the conduction band or to electron scavengers [17]. Furthermore, Nakamura et al. showed that the photo-excitation from the nitrogen doping level located at ca.+0.75 eV above valence band to the conduction band [18].

Many kinds of nitrogen sources have been used for the preparation of N–TiO_2, including urea, sulfur urine, tri-ethylamine ammonia ammonium chloride and ammonium nitrate [9]. It is feasible that doping (nitrogen) elements into the TiO_2 nanopowders can achieve high photocatalytic activity under visible

* Corresponding author. Tel.: +86 86283008.
E-mail addresses: hanlei-0517@163.com (L. Han), hlliu2002@163.com (H. Liu).

0304-3894/$ – see front matter © 2009 Elsevier B.V. All rights reserved.
doi:10.1016/j.jhazmat.2009.10.037

light. However, the separation problems of TiO_2 powder hold back its utilization in wastewater treatment [9,19]. Therefore, many kinds of TiO_2 films on various substrates were used to substitute TiO_2 nanopowders as photocatalyst, such as glass, hydrophobic montmorillonite, zeolite, activated carbons, stainless steel, foamed aluminum, etc [20–25]. Fortunately, the fabrication of TiO_2 film by an anodic oxidation provides a unique opportunity for the photocatalysis application. In-situ anodic oxidation has been a new focus in photocatalytic filed, which may be carried out conveniently.

We have successfully fabricated TiO_2/Ti photoelectrodes based on in situ growth of TiO_2 film on titanium substrate in previous research [26]. In order to promote the visible light response we carried out the synthesis of well-performed N-doped anodization TiO_2/Ti photoelectrode at low temperature by plasma based ion implantation (PBII). To the best of our knowledge, there has not yet been any report on N-doped TiO_2/Ti photoelectrode by PBII.

In this paper, the crystal structure, electrochemical properties, and photoelectrocatalytic activity of N–TiO_2/Ti photoelectrode by PBII were investigated. The electrode was characterized by SEM, AFM, XRD, XPS, UV/vis/DRS and surface photovoltage spectroscopy (SPV), as well as photoelectrochemical measurements. Photocatalytic activity of the N-doped TiO_2/Ti photoelectrodes was evaluated using Rhodamine B (Rh.B) solution as the objective substance. It is of significant importance to the TiO_2 photocatalyst for practical applications.

2. Experimental methodology

2.1. Materials and instruments

Titanium plate (purity > 99.5%) was purchased from Baoji Titanium and Nickel Manufacture Ltd. Company, China. The experimental solution prepared with doubly distilled water. Other chemicals were of analytical reagent grade and used without further purification.

Scanning electronic microscopy (SEM) images were obtained to characterize the surface morphology and pore distribution by D/max-rB SEM. Atomic force microscopy (AFM) images were obtained using DI D-3100 AFM (USA). X-ray diffraction (XRD) spectra were obtained using a Rigaku D/max-γB diffractometer with Cu Kα radiation (λ = 1.5417 Å).

The surface composition and bonding of the films were detected by an X-ray photoelectron spectrometry (XPS, PHI 5700 ESCA system spectrometer) using Al-Kα X-ray (1486.6 eV) at 15 kV and 100 W. The binding energy was referenced to the C 1s line at 284.8 eV for calibration. Ultra violet/visible light diffuse reflectance spectra (UV/vis/DRS) spectra with a wavelength range of 200–800 nm were recorded at room temperature using a Lambda 900 UV–vis–DRS spectroscopy with a diffuse reflectance accessory, and pure TiO_2 were used as references. The surface photovoltage spectroscopy (SPV) was tested in Jilin University. Photoelectrochemical performance was investigated using a CHI EC analyzer (a Model 263A Potentiostat/Galvamastat, America) in a standard three electrode configuration with the N-doped TiO_2 photoelectrode (1 cm^2) as a photo-anode, Pt foil as the counter electrode, and a saturated calomel electrode (SCE) as the reference electrode. 35 W HID Xenon light (Germany) was used as the light source with a distance of 3 cm from the anode. All the experiments were performed at room temperature.

2.2. Experimental installation

As shown in Fig. 1, the main components were the cylindrical quartz cell of 25 mm in diameter and 50 mm in height. The reactor contained a N-doped TiO_2/Ti photoelectrode, the working electrode (WE), used as the anode and a Pt plate of 50 mm in length and 20 mm in width, the auxiliary electrode (AE), used as the cathode. 35 W HID Xenon light was positioned against the reactor, facing the N-doped TiO_2/Ti photoelectrode. A potentiostat (Sanke limited company, Shanghai) was used to provide a potential bias between the anode and cathode.

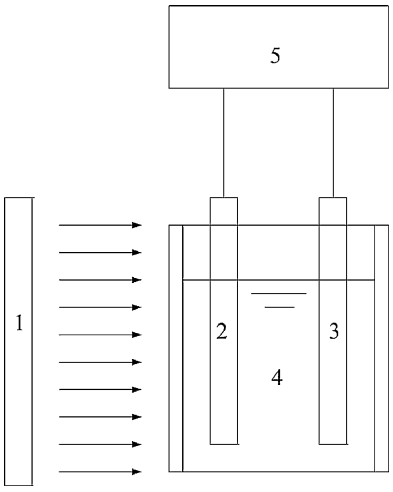

Fig. 1. Schematic diagram of the reactor for photoelectrocatalytic oxidation: (1) Xe lamp; (2) N-doped TiO_2/Ti photoelectrodes (anode); (3) Pt cathode; (4) reactor; (5) potentiostat.

2.3. Preparation of N-Doped TiO_2/Ti photoelectrode

TiO_2/Ti photoelectrode based on Ti substrate was fabricated according to the method reported in the literature with a little modification. Titanium sheet of 0.50 mm thickness was used as the substrate. Prior to anodic oxidation, the titanium sheet was mechanically polished with different emery papers to a mirror-like finish. Then the polished titanium was e ultrasonically cleaned in deionized water for 20 min, and subsequently it was chemically etched by immersing in a mixture of $HF/HNO_3/H_2O$ (1:4:5 in volume) for 30 s and rinsed by deionized water carefully. Finally the as-prepared TiO_2/Ti photoelectrode was dried at room temperature.

The TiO_2/Ti photoelectrodes were made by anodization in a two-electrode EC cell with a solution of 0.5 mol/L H_2SO_4 with a Ti sheet serving as the anode and copper sheet serving as the cathode. All the anodization experiments were performed at room temperature. Anodization was done in two steps: (1) the current density was kept at 100 mA/cm^2 from the beginning of the oxidation until the voltage reached 160 V; (2) the voltage of anodization (160 V) was kept constant until the current density decreased to 36 mA/cm^2. The whole anodization process lasted for 10 min. After the anodization, the sample was immediately rinsed with deionized water. N ion was implanted by PBII (self-made by Harbin University) under 200 °C. The schematic of PBII was shown in Fig. 2.

2.4. Photoelectrocatalytic activity evaluation of N-doped TiO_2/Ti photoelectrodes

The PC and PEC performance of N-doped TiO_2/Ti photoelectrodes was investigated in aqueous solution using Rh.B as a target pollutant in a single photoelectrochemical compartment.15 mL of Rh.B solution (5 mg/L) was added into the quartz reactor. The PEC degradation experiments were investigated with 35 W HID xenon light simulated solar light. The irradiation lasted for 2 h. The degradation of Rh.B was analyzed using a 752 spectrophotometer at wavelength of 552 nm.

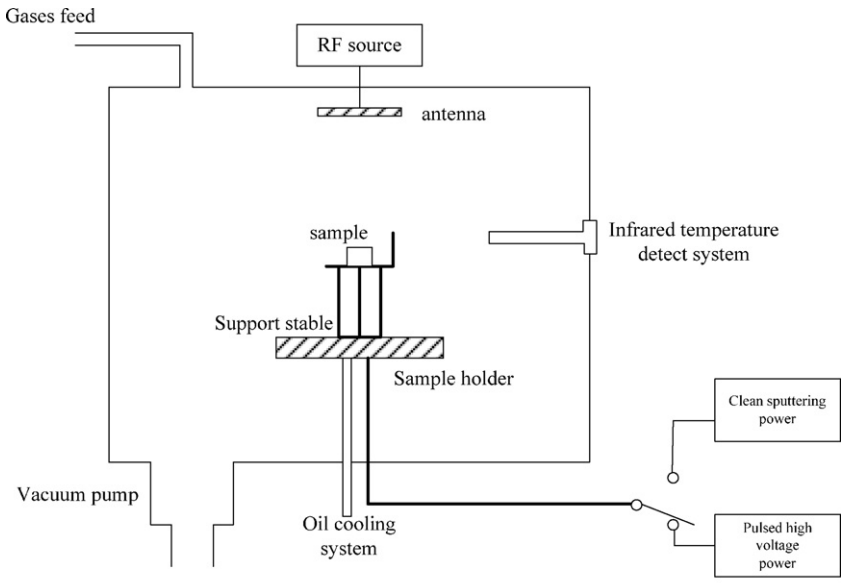

Fig. 2. The schematic of plasma based ion implantation.

The degradation of Rh.B was calculated using the following formula:

$$D(\%) = \frac{(C_0 - C)}{C_0} \times 100\%$$

where C_0 is the initial concentration; C is the concentration after a certain period of illumination time.

3. Results and discussion

3.1. Characterizations of N-doped TiO_2/Ti photoelectrodes

3.1.1. Surface morphology of N-doped TiO_2/Ti photoelectrodes

SEM was employed for the morphological characterization of the TiO_2 photoelectrodes, as shown in Fig. 3. The surface topography and roughness were also investigated by atomic force microscopy (AFM). The AFM images of N-doped TiO_2/Ti photoelectrodes are shown in Fig. 4.

Apparently, TiO_2/Ti photoelectrodes showed gray color, while N-doped TiO_2/Ti photoelectrode were light yellow. Both images clearly demonstrate that the anodization film displayed a rough and porous surface.

Therefore, it can be concluded that the N-doped TiO_2/Ti photoelectrode had much more microporous and larger roughness than undoped TiO_2. The dia of N-TiO_2/Ti was 103.88 nm, while undoped one was 80.39 nm. More microporous and larger roughness indicated that the N-doped TiO_2/Ti photoelectrode had larger specific surface area and more active sites, thus, might present higher adsorption capacity and promote its photocatalytic activity.

3.1.2. XRD analysis of N-doped TiO_2/Ti photoelectrode

The crystal structure significantly influenced the photocatalytic activity of TiO_2 photoelectrode. Amorphous crystal showed little photocatalytic activity due to crystal defect state, i.e. the unbonded oxygen, might become the recombination centre of photoelectron and hole.

Fig. 5 is the XRD patterns of the undoped TiO_2 and N-doped TiO_2 photoelectrodes. The patterns showed that the films were mainly composed of anatase phase and rutile phase. The crystal of undoped and N-doped TiO_2 photoelectrodes showed little difference. None of N-peak was observed most probable that the amount of doped nitrogen is low and this element entered the crystal lattice of TiO_2.

The average crystal size can be calculated by the Scherrer's formula, i.e. $D = 0.89\lambda/\beta\cos\theta$, where D is the crystal size, λ is the wavelength of X-ray radiation, β is the line width at half-maximum (FWHM) and θ is Bragg angle.

On the basis of the Scherrer's formula, the average crystal sizes of the N-doped and non-doped TiO_2 photoelectrodes were calculated

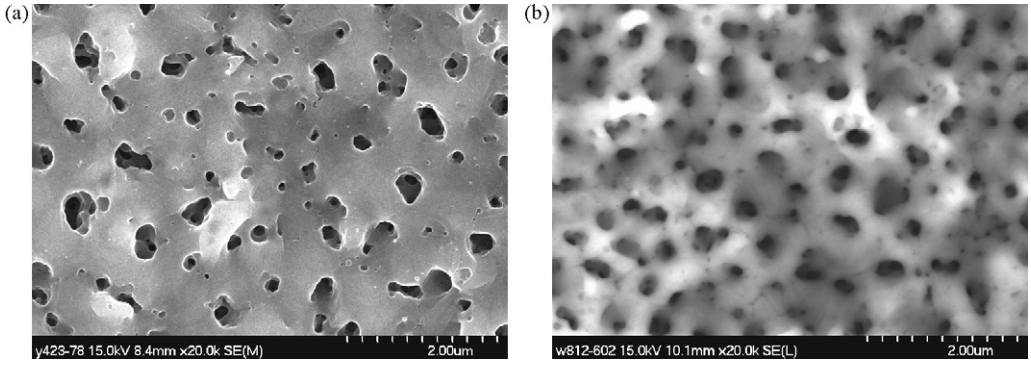

Fig. 3. SEM images of photoelectrodes: (a) TiO_2/Ti photoelectrodes; (b) N-doped TiO_2/Ti photoelectrodes.

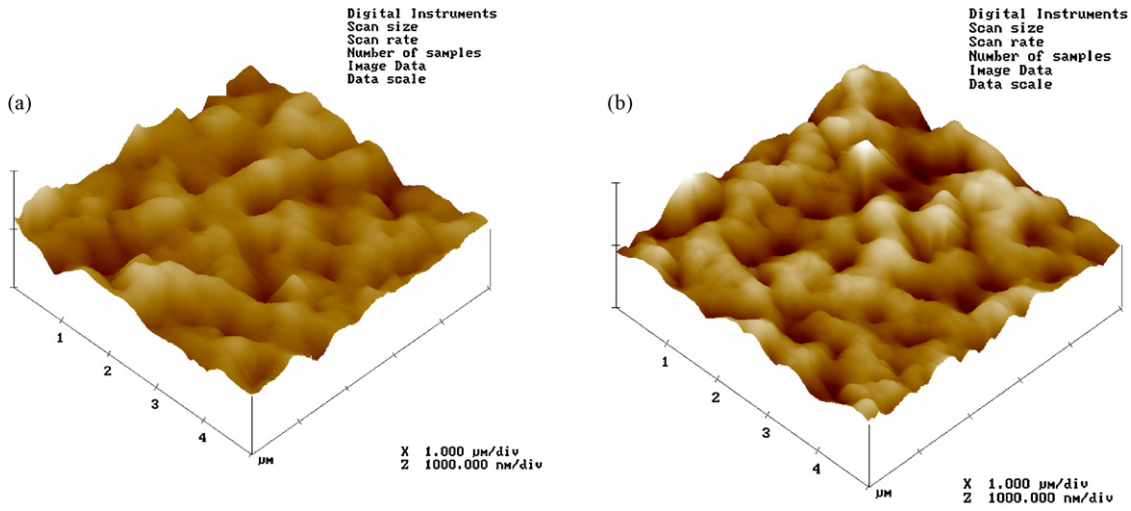

Fig. 4. AFM images of photoelectrodes: (a) TiO_2/Ti photoelectrodes; (b) N-doped TiO_2/Ti photoelectrodes.

to be ~24 and ~32 nm, respectively. It indicated that the incorporation of nitrogen into the film of TiO_2 could hinder the growth of crystalline particles.

An effective method of enhancing the photocatalytic activity is to hinder the recombination of photo-generated electro and hole pairs. The particle diameter may influence the photochemical and electrochemical properties of catalyst. Smaller size can facilitate the separation of charge carriers.

3.1.3. XPS analysis of N-TiO_2/Ti photoelectrode

Investigation of the oxidation state of the nitrogen dopant was carried out by XPS. Fig. 6 is the XPS full-scale pattern of N-doped TiO_2/Ti, which shows that the N-doped TiO_2 film contained four peaks, including Ti 2p, O 1s, N 1s and C 1s. Among them, Ti and O were main contents, while C could be ascribed to the residual carbon from the precursor solution and the adventitious hydrocarbon from the XPS instrument itself. Figs. 7 and 8 were high resolution spectrum of Ti 2p and O 1s. The results revealed that the titanium was mainly at Ti^{4+} while the O element existed as two kinds of chemical states involving the crystal lattice oxygen and adsorbed oxygen.

Compared with the undoped TiO_2, the O 1s peak of N-doped TiO_2 film slightly shifted toward higher binding energy and the Ti

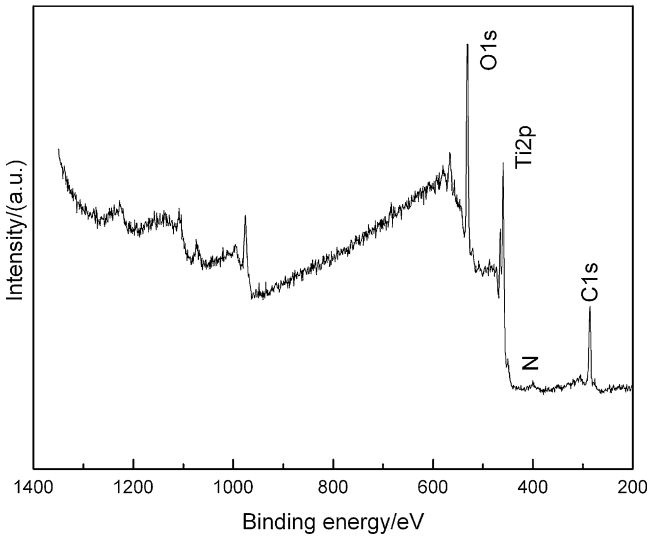

Fig. 6. XPS spectrum of N-doped TiO_2/Ti.

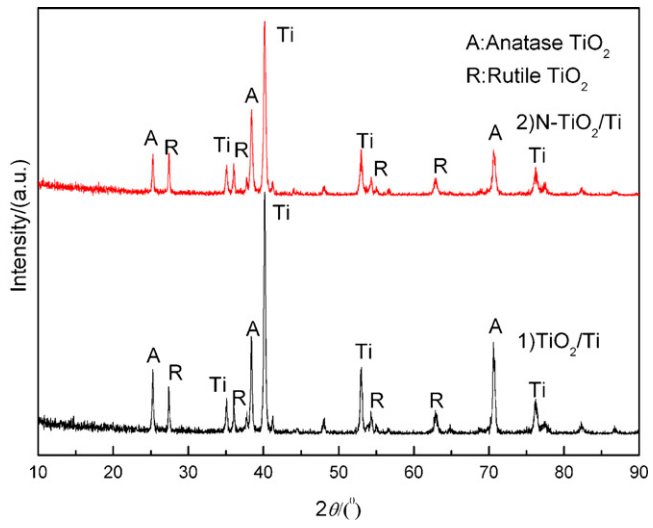

Fig. 5. The X-ray diffraction pattern of undoped and N-doped TiO_2 electrodes.

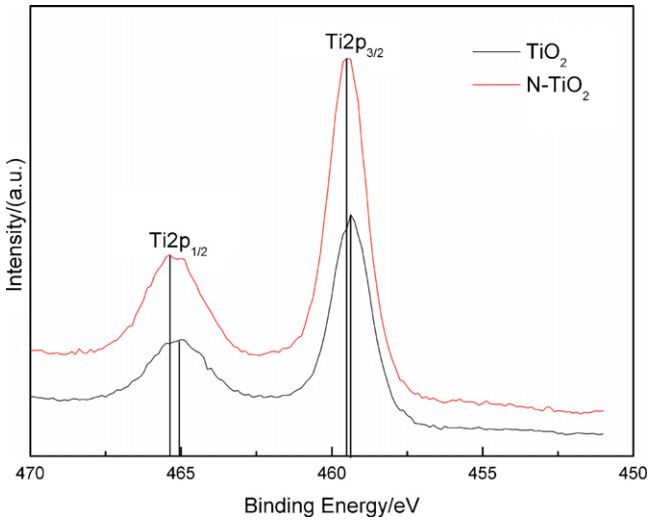

Fig. 7. Ti 2p XPS spectrum of N-doped TiO_2/Ti.

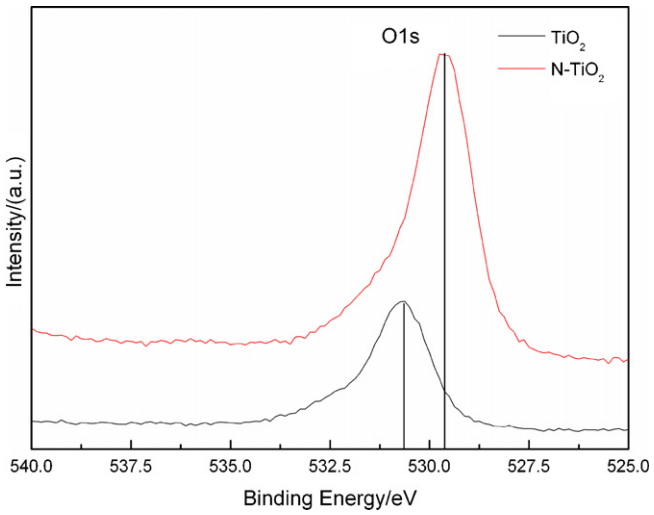

Fig. 8. O 1s XPS spectrum of N-doped TiO_2/Ti.

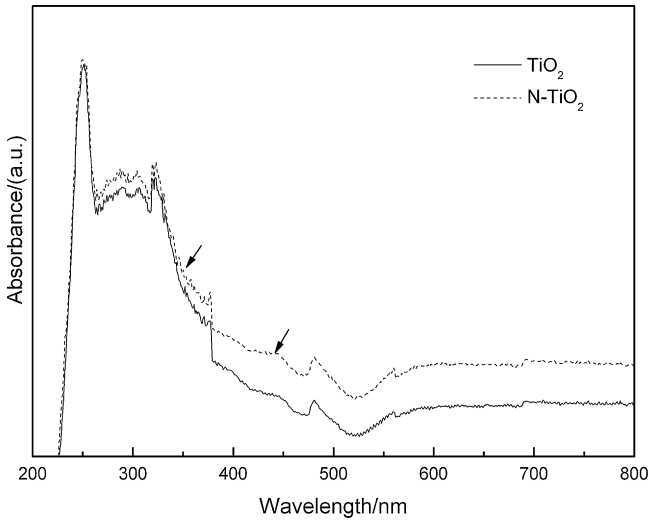

Fig. 10. UV/vis/DRS spectra of N-doped and undoped TiO_2/Ti.

2p peak slightly shifted toward lower binding energy, respectively. The shifting might be resulted from the fact that some of oxygen of O–Ti–O was substituted with nitrogen to form O–Ti–N.

Fig. 9 shows the XPS spectra for the N 1s region of N-doped TiO_2 and its fitting curves. There is a broad peak observed from 397 to 403 eV. Three well-defined peaks can be distinguished, which indicated the N 1s binding energies were 401.88, 399.75, 395.59 eV, respectively. Usually the peak at 396 eV could be assigned to an atomic β-N state (for example in TiN) and the one at 400 eV could be assigned to a well-screened γ-N state (essentially adsorbed N), while the one at 396-400 eV was ascribed to a O–Ti–N state, which was in agreement with the findings reported by Chen and Burda [27] and Valentin et al. [28]. According to Valentin et al., the N 1s peak is possibly due to a variety of substitutional (O–Ti–N) and/or interstitial (NO, NO_2 or NH_x) nitrogen species in the TiO_2 matrix. Therefore, one can deduce from XPS results that nitrogen was not only successfully implanted in the structure but it was also present in a chemically bonded state, indicating that this type of nitrogen was the active doping species.

3.1.4. Photo absorption performance of N–TiO_2/Ti photoelectrode

The UV/vis/DRS of TiO_2 photoelectrodes are presented in Fig. 10. In the UV light region, the absorption intensity of the N-doped sample was increased significantly which indicated that the N-doped TiO_2 photoelectrode was more sensitive to UV light than that of the non-doped one. Moreover, an additional edge in the visible range is present. In the meantime, a shift of the absorption threshold toward the visible light region was observed for the N-doped sample. The absorption of visible lights of N–TiO_2 is due to the excitation of electrons from localized N-doping level in the band gap [29]. The valence band of N–TiO_2 consisted of N 2p and O 2p, that is, only donor energy states existed in the band of N–TiO_2. As a result, the recombination probability of hole–electron pairs was reduced largely [30]. The DRS results signified that the N entered into the atomic lattice of TiO_2 might decrease the band gap and thus had a red shift in UV–vis absorption band, which might promote the PC activity of TiO_2 film. Consequently, a higher solar light response of the N-doped TiO_2/Ti photoelectrode than the non-doped one might be exhibited as suggested by the UV/vis/DRS spectra.

3.1.5. SPV analysis of N-TiO_2/Ti photoelectrode

SPV spectroscopy is a good tool for studying photogenerated charge carriers in nanostructured materials [31]. It can detect an optical absorption spectrum by the illumination-induced change in the surface potential due to the drift, accumulation, and recombination of photogenerated carriers. It is generally accepted that the higher SPV signal suggests the higher separation rate of photogen-

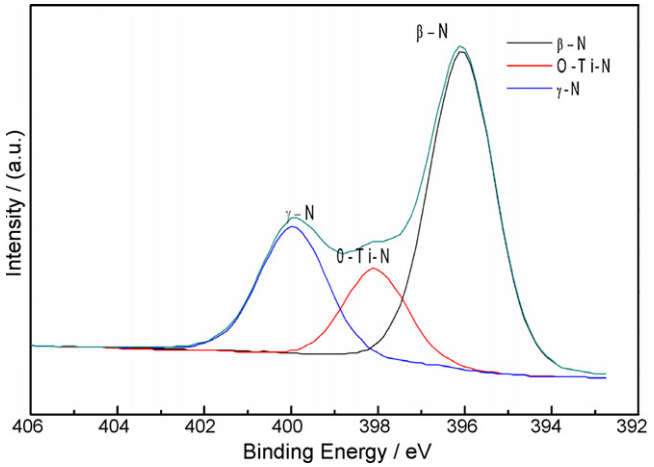

Fig. 9. N 1s XPS spectrum of N-doped TiO_2/Ti.

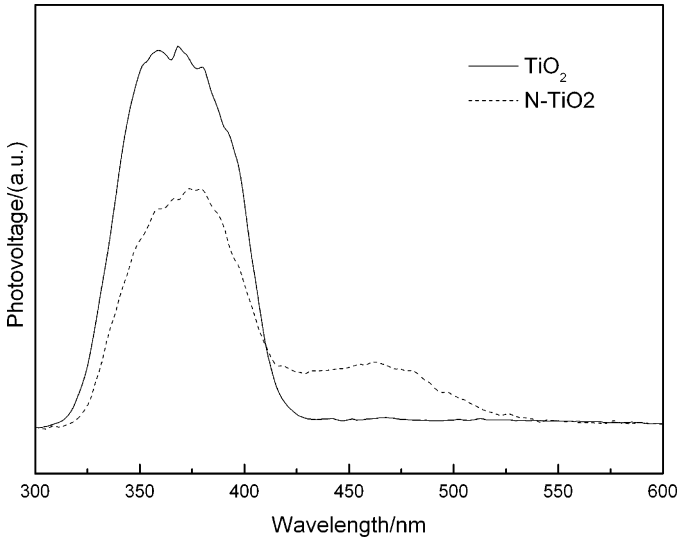

Fig. 11. SPV spectra of N-doped TiO_2/Ti and undoped photoelectrode.

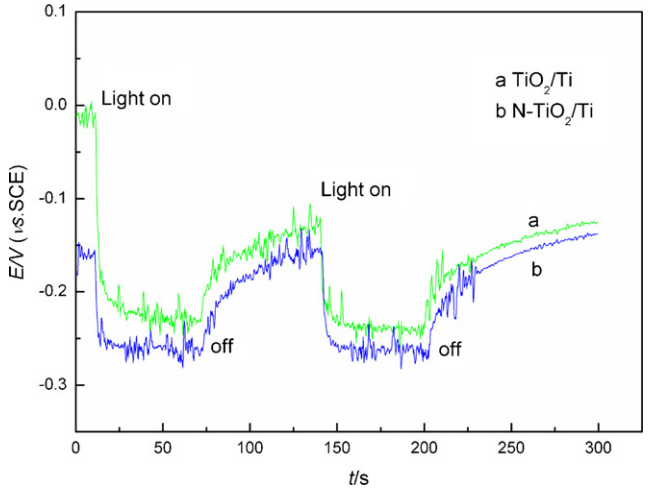

Fig. 12. Open-circuit photovoltage vs. time curves of N–TiO_2/Ti photoelectrode.

erated charge carriers. The SPV spectra of N-doped and undoped TiO_2/Ti are shown in Fig. 11. N-doped TiO_2/Ti photoelectrode displayed a much higher SPV signal than that of TiO_2/Ti. Considering the analysis in Fig. 11, this result proved our assumption, that is, an elevated photocurrent density was obtained on the N-doped photoelectrode due to its higher light response in the visible light region. The obtained results are in agreement with those of the DRS analysis, demonstrating that the N-doped TiO_2 film prepared by ion implanting was suitable to be utilized in visible light region.

3.2. Photoelectrochemical properties of N–TiO_2/Ti electrode

3.2.1. Open-circuit photovoltage (OCP) analysis

The photovoltage had also been measured under open-circuit condition to investigate photoresponse of N–TiO_2/Ti photoelectrode. The photovoltaic response was an important parameter for the characterization of photoresponse activity. A higher photovoltage means a more possible accumulation of photo-generated electrons on the conduction band of titania. Once light source was turned on, the potential immediately negatively shifted under white light irradiation and switched back promptly to less negative values than its rest potential due to fast charge recombination after the light was cut off. It meant that most of excited photoelectrons transferred and accumulated on the conduction band of TiO_2, which accordingly contributed to the formation of the space charge layers along the pore channels. When light was off, this potential gradually increased up to the initial value again. It indicated that these conduction band electrons must have suffered relaxation decay through a recombination process with cationic radicals, which was ascribed to a strong electric field distribution within the depletion layers.

A comparison of the response of the OCP of the N–TiO_2/Ti photoelectrode and the TiO_2/Ti photoelectrode, respectively, with and without light illumination is depicted in Fig. 12. Herein the photosensitization response of the two photoanodes exhibited a similar varying tendency. However, the N–TiO_2/Ti photoelectrode displayed a higher photovoltaic response rather than the undoped photoelectrode. It suggested that a more effective separation of photo-generated electrons and holes, a higher photosensitization activity and quantum efficiency could be achieved for the N–TiO_2/Ti photoelectrode, which was consistent with the SPV results.

3.2.2. Photocurrent measurements

The transient photocurrent spectra are generally acknowledged as an effective parameter for the properties of light-induced interface charge transfer between the interface of electrode and solution [32]. Fig. 13 depicts the transient photocurrent spectra of N–TiO_2/Ti photoelectrode in 0.5 mol/L Na_2SO_4 at a sequence of applied potential increased from −0.2 to 0.4 V.

As illustrated in Fig. 13, N–TiO_2/Ti photoelectrode showed different effects of bias potential on photocurrent. Under illumination when the applied potential increased from −0.2 to 0.4 V, the photocurrent density of N–TiO_2/Ti photoelectrode increased rapidly, which accounted for that with the increase of applied positive potential, the Fermi level decreased and the driving force for separation of holes and electrons increased. This demonstrated that the recombination of photogenerated electrons and holes decreased, which was in accordance with the SPV measurements, thus the photoelectrochemical activity of N–TiO_2/Ti photoelectrode was promoted. Under the condition of light off, the transient photocurrent decreased with the applied potential shifting from 0 to −0.2 V, meanwhile, a minor reverse photocurrent appeared. It illustrated that the negative potential was harmful for the separation of photogenerated electrons and holes and the carriers entered into the electrolyte solution and formed cathode photocurrent when the light turned off.

3.2.3. Comparison of photocurrent

The magnitude of the anodic photocurrent was proportional to the number of the photogenerated electrons that transferred into the outer circuit. A more effective charge transport would result in a larger photocurrent density. The photocurrent–time curves of N–TiO_2/Ti photoelectrode and TiO_2/Ti photoelectrode are shown in Fig. 14. As shown in this figure, the N–TiO_2/Ti photoelec-

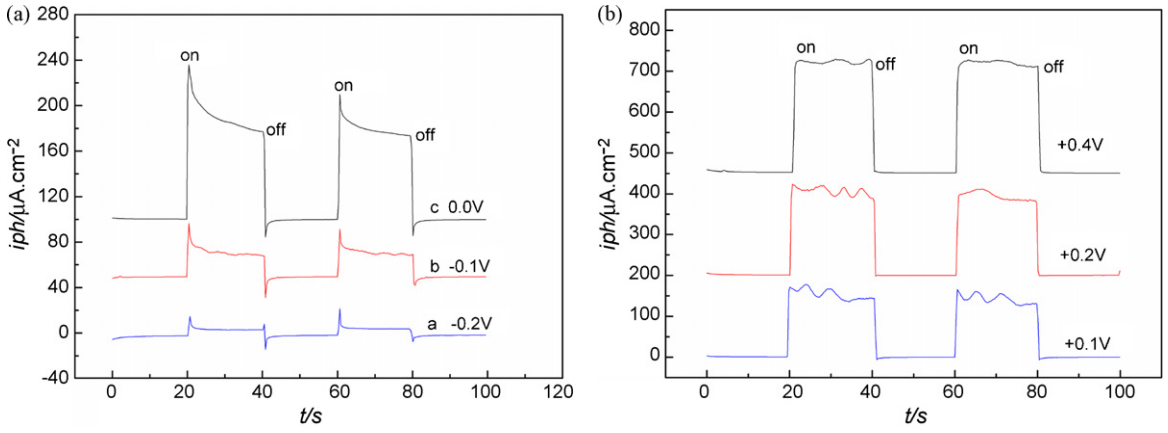

Fig. 13. Transient photocurrent spectra of N–TiO_2/Ti photoelectrode: (a) negative bias and (b) positive bias.

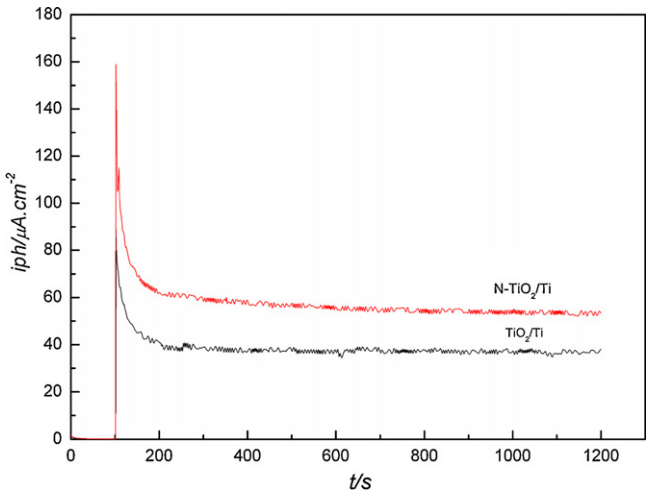

Fig. 14. The photocurrent–time curve of N–TiO_2/Ti and TiO_2/Ti photoelectrode.

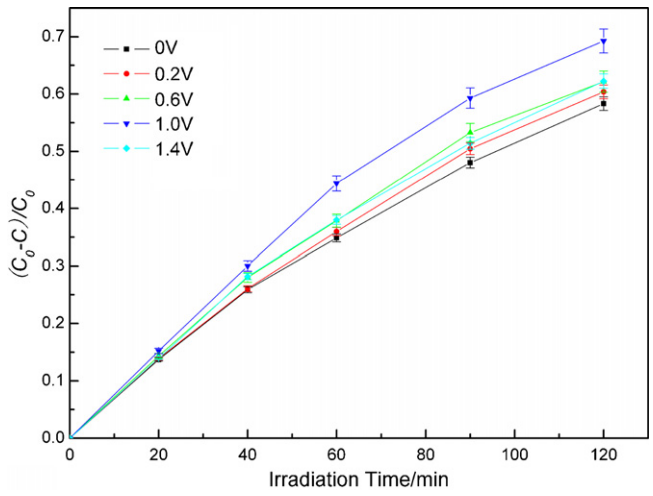

Fig. 16. PEC effect of N-doped photoelectrode vs. bias potential.

trode produced an anodic photocurrent density about 60 μA/cm^2, which was 1.5 times higher than that of TiO_2/Ti photoelectrode. The improved photocurrents indicated clearly that the N–TiO_2/Ti photoelectrode was more favorable for the transport of the photo-generated electrons than TiO_2/Ti photoelectrode, which indicated the N–TiO_2/Ti photoelectrode might have higher photochemical activity.

3.3. PC performance under different nitrogen content

The N–TiO_2/Ti photoelectrodes were prepared in different conditions of nitrogen ion implantation voltage, i.e. −30 and −50 kV, with the doping content of 4×10^{15} and 8×10^{15} N/cm^2, respectively. The degradation efficiency of Rh.B under visible light on the different phototelectrodes is displayed in Fig. 15. It is directly seen from this figure that the Rh.B removal rate on the N-doped TiO_2 photoelectrode was faster than that on the non-doped one. After 2-h xenon-lamp irradiation, 58.3% of Rh.B was degraded on the N-doped photoelectrode, i.e. 1.94×10^{-5} mM min^{-1} cm^{-2}, whose doping content was 4×10^{15} N/cm^2, while ca. 46% of Rh.B was removed by the undoped TiO_2 electrode, i.e.1.53×10^{-5} mM min^{-1} cm^{-2}.

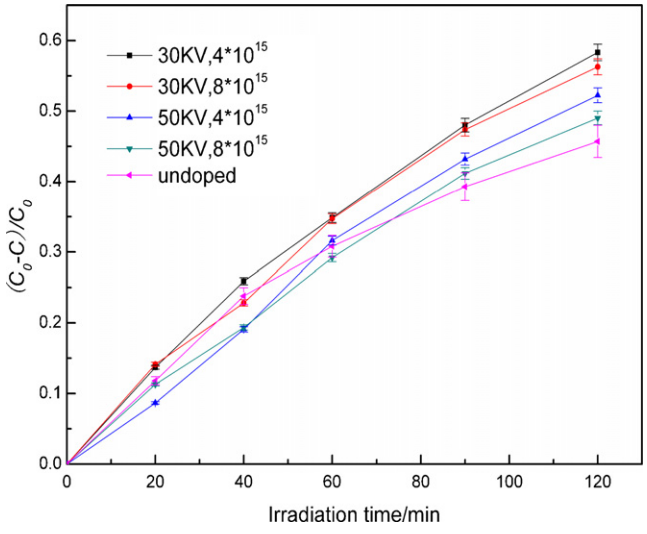

Fig. 15. Rh.B removal rate on the N-doped TiO_2 photoelectrode under different nitrogen content.

3.4. PEC performance of N-doped photoelectrode under different bias potential

Fig. 16 shows the variation of Rh.B removal on N-doped TiO_2/Ti photoelectrode, whose doping content was 4×10^{15} N/cm^2, as a function of the applied bias potential and xenon-lamp irradiation time. The result showed that the applied bias potential can improve the photocatalytic efficiency of N-doped TiO_2/Ti photoelectrode. When the applied potential was 1 V, the removal ratio of Rh.B reached 69%, i.e.2.31×10^{-5} mM min^{-1} cm^{-2}, which was higher than those of 0.6 and 1.4 V. This could be attributed to the reason that the applied bias potential might drive photogenerated electrons to the cathode through external circuit, thus would accelerate the separation of photo-generated carriers [33] and promote the photocatalytic efficiency.

3.5. Comparison of PEC performance of N-TiO_2/Ti and TiO_2/Ti photoelectrodes

Fig. 17 shows the variation of Rh.B removal on N-TiO_2/Ti photoelectrode in the conditions of doping content 4×10^{15} N/cm^2, applied bias potential 0.6 and 1.0 V, and xenon-lamp irradiation, as well as the removal on undoped photoelectrode. The result suggested that the applied bias potential could improve the PEC efficiency, which was consistent with the results of

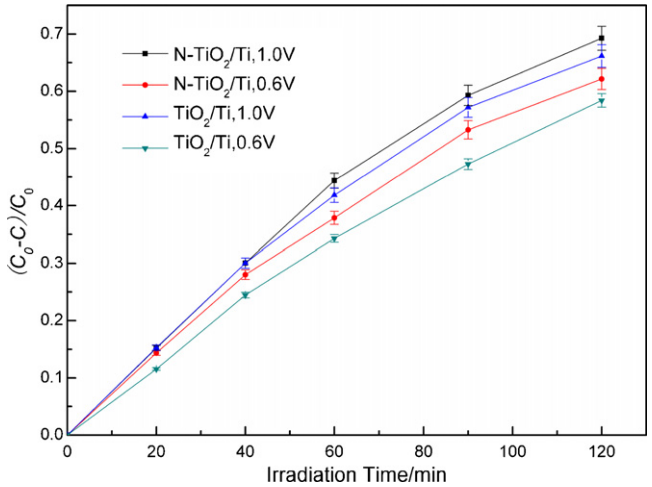

Fig. 17. Rh.B degradation of N–TiO_2/Ti and pure TiO_2/Ti photoelectrodes.

photochemical characterization. The Rh.B removal ratio on the N-doped TiO_2 photoelectrode was ca.3% higher than that of undoped photoelectrode.

4. Conclusions

The N–TiO_2/Ti photoelectrodes had been prepared successfully by the process of anodization and subsequent nitrogen doping by plasma based ion implantation (PBII) technology. The photocatalytic performance of as-prepared N-TiO_2/Ti photoelectrode was better when the nitrogen injection was carried out on the voltage −30 kV, nitrogen doping content of 4×10^{15} N/cm^2. Under visible light, the Rh.B photocatalytic degradation ratio of N-doped TiO_2/Ti photoelectrode increased 12% compared with TiO_2. In addition, the photoelectrochemical efficiency of N-doped TiO_2/Ti photoelectrode was ca. 3% higher than that of undoped TiO_2.

Acknowledgements

This work was supported by National Natural Science Foundation of China (No. 50678044), National Creative Research Groups of National Natural Science Foundation of China (No. 50821002) and State Key Laboratory of Urban Water Resources and Environment (No. 2008DX06).

References

[1] M. Tamimi, S. Qourzal, A. Assabbane, J.M. Chovelon, C. Ferronato, Y. Ait-Ichou, Photocatalytic degradation of pesticide methomyl: determination of the reaction pathway and identification of intermediate products, Photochem. Photobiol. Sci. 5 (2006) 477–482.
[2] Y.M. Lin, Y.H. Tseng, J.H. Huang, C.C. Chao, C.C. Chen, I. Wang, Photocatalytic activity for degradation of nitrogen oxides over visible light responsive titania-based photocatalysts, Environ. Sci. Technol. 40 (2006) 1616–1621.
[3] D.Z. Li, Z.X. Chen, Y.L. Chen, W.J. Li, H.J. Huang, Y.H. He, X.Z. Fu, A new route for degradation of volatile organic compounds under visible light: using the bifunctional photocatalyst Pt/$TiO_{2-x}N_x$ in H_2–O_2 atmosphere, Environ. Sci. Technol. 42 (2008) 2130–2135.
[4] A. Kar, Y.F. Smith, V.R. Subramanian, Improved photocatalytic degradation of textile dye using titanium dioxide nanotubes formed over titanium wires, Environ. Sci. Technol. 43 (2009) 3260–3265.
[5] J.A. Rengifo-Herrera, K. Pierzchata, A. Sienkiewicz, L. Forró, J. Kiwi, C. Pulgarin, Abatement of organics and *Escherichia coli* by N, S co-doped TiO_2 under UV and visible light. Implications of the formation of singlet oxygen ($^1O_2$) under visible light, Appl. Catal. B: Environ. 88 (2009) 398–406.
[6] G. Li, T. An, J.X. Chen, G.Y. Sheng, J.M. Fu, F.Z. Chen, S.Q. Zhang, H.J. Zhao, Photoelectrocatalytic decontamination of oilfield produced wastewater containing refractory organic pollutants in the presence of high concentration of chloride ions, J. Hazard. Mater. B 138 (2006) 392–400.
[7] Y. Irokawa, T. Morikawa, K. Aoki, S. Kosaka, T. Ohwaki, Y. Taga, Photodegradation of toluene over $TiO_{2-x}N_x$ under visible light irradiation, Phys. Chem. Chem. Phys. 8 (2006) 1116–1121.
[8] R. Asahi, T. Morikawa, T. Ohwaki, K. Aoki, Y. Taga, Visible-light photocatalysis in nitrogen-doped titanium oxides, Science 293 (2001) 269–271.
[9] M.Y. Xing, J.L. Zhang, F. Chen, New approaches to prepare nitrogen-doped TiO_2 photocatalysts and study on their photocatalytic activities in visible light, Appl. Catal. B: Environ. 89 (2009) 563–569.
[10] F.B. Li, X.Z. Li, M.F. Hou, K.W. Cheah, W.C.H. Choy, Enhanced photocatalytic activity of Ce^{3+}–TiO_2 for 2-mercaptobenzothiazole degradation in aqueous suspension for odour control, Appl. Catal. Gen. A 285 (2005) 181–189.
[11] Y.H. Zhang, H.X. Zhang, Y.X. Xu, Y.G. Wang, Europium doped nanocrystalline titanium dioxide: preparation, phase transformation and photocatalytic properties, J. Mater. Chem. 13 (2003) 2261–2265.
[12] Y.B. Xie, X.Z. Li, Degradation of bisphenol A in aqueous solution by H_2O_2-assisted photoelectrocatalytic oxidation, J. Hazard. Mater. B 138 (2006) 526–533.
[13] W.T. Sun, Y. Yu, H.Y. Pan, X.F. Gao, Q. Chen, L.M. Peng, CdS quantum dots sensitized TiO_2 nanotube-array photoelectrodes, J. Am. Chem. Soc. 130 (2008) 1124–1125.
[14] J.M. Macák, H. Tsuchiya, A. Ghicov, P. Schmuki, Dye-sensitized anodic TiO_2 nanotubes, Electrochem. Commun. 7 (2005) 1133–1137.
[15] T.C. Jagadale, S.P. Takale, R.S. Sonawane, H.M. Joshi, S.I. Patil, B.B. Kale, S.B. Ogale, N-doped TiO_2 nanoparticle based visible light photocatalyst by modified peroxide sol–gel method, J. Phys. Chem. C 112 (2008) 14595–14602.
[16] M. Pelaez, A.A. Cruz, E. Stathatos, P. Falaras, D.D. Dionysiou, Visible light-activated N–F-codoped TiO_2 nanoparticles for the photocatalytic degradation of microcystin-LR in water, Catal. Today 144 (2009) 19–25.
[17] S. Livraghi, M.C. Paganini, E. Giamello, A. Selloni, C.D. Valentin, G. Pacchioni, Origin of photoactivity of nitrogen-doped titanium dioxide under visible light, J. Am. Chem. Soc. 128 (2006) 15666–15671.
[18] R. Nakamura, T. Tanaka, Y. Nakato, Mechanism for visible light responses in anodic photocurrents at N-Doped TiO_2 film electrodes, J. Phys. Chem. B 108 (2004) 10617–10620.
[19] S. Higashimoto, M. Azuma, Photo-induced charging effect and electron transfer to the redox species on nitrogen-doped TiO_2 under visible light irradiation, Appl. Catal. B: Environ. 89 (2009) 557–562.
[20] Y.J. Chen, E. Stathatos, D.D. Dionysiou, Microstructure characterization and photocatalytic activity of mesoporous TiO_2 films with ultrafine anatase nanocrystallites, Surf. Coat. Technol. 202 (2008) 1944–1950.
[21] T.C. An, J.X. Chen, G.Y. Li, X.J. Ding, G.Y. Sheng, J.M. Fu, B.X. Mai, K.E. O'Shea, Characterization and the photocatalytic activity of TiO_2 immobilized hydrophobic montmorillonite photocatalysts degradation of decabromodiphenyl ether (BDE 209), Catal. Today 139 (2008) 69–76.
[22] M.L. Huang, C.F. Xu, Z.B. Wu, Y.F. Huang, J.M. Lin, J.H. Wu, Photocatalytic discolorization of methyl orange solution by Pt modified TiO_2 loaded on natural zeolite, Dyes Pigments 77 (2008) 327–334.
[23] X.J. Wang, Y.F. Liu, Z.H. Hu, Y.J. Chen, W. Liu, G.H. Zhao, Degradation of methyl orange by composite photocatalysts nano-TiO_2 immobilized on activated carbons of different porosities, J. Hazard. Mater. 169 (2009) 1061–1067.
[24] Y.J. Chen, D.D. Dionysiou, TiO_2 photocatalytic films on stainless steel: the role of Degussa P-25 in modified sol–gel methods, Appl. Catal. B: Environ. 62 (2006) 255–264.
[25] H. Chen, S.W. Lee, T.H. Kim, B.Y. Hur, Photocatalytic decomposition of benzene with plasma sprayed TiO2-based coatings on foamed aluminum, J. Eur. Ceram. Soc. 26 (2006) 2231–2239.
[26] X.Z. Li, H.L. Liu, P.T. Yue, Photoelectrocatalytic oxidation of rose bengal in aqueous solution using a Ti/TiO_2 mesh electrode, Environ. Sci. Technol. 34 (2000) 4401–4406.
[27] X.B. Chen, C. Burda, Photoelectron spectroscopic investigation of nitrogen-doped titania nanoparticles, J. Phys. Chem. B 108 (2004) 15446–15449.
[28] C.D. Valentin, G. Pacchioni, A. Selloni, S. Livraghi, E. Giamello, Characterization of paramagnetic species in N-Doped TiO_2 powders by EPR spectroscopy and DFT calculations, J. Phys. Chem. B 109 (2005) 11414–11419.
[29] D.M. Chen, Z.Y. Jiang, J.Q. Geng, Q. Wang, D. Yang, Carbon and nitrogen co-doped TiO_2 with enhanced visible-light photocatalytic activity, Ind. Eng. Chem. Res. 46 (2007) 2741–2746.
[30] Z.Q. Liu, Y.P. Zhou, Z.H. Li, Y.C. Wang, C.C. Ge, Preparation and characterization of (metal, nitrogen)-codoped TiO_2 by $TiCl_4$ sol–gel auto-igniting synthesis, Rare Met. 26 (2007) 263–270.
[31] K. Sakai, S. Oyama, K. Noguchi, A. Fukuyama, T. Ikari, T. Okada, Optical properties of nanostructured ZnO crystal synthesized by pulsed-laser ablation, Phys. E 40 (2008) 2489–2493.
[32] H. Li, S.W. Yao, W.G. Zhang, Z.H. Wang, Y.H. Pen, Photoelectrochemical properties of TiO_2 nanotube arrays electrodes, Rare Met. Mate. Eng. 36 (2007) 1749–1753.
[33] Y. Ku, Y.C. Lee, W.Y. Wang, Photocatalytic decomposition of 2-chlorophenol in aqueous solution by UV/TiO_2 process with applied external bias voltage, J. Hazard. Mater. B 138 (2006) 350–356.